

# Energy Optimization of Wind Turbines via a Neural Control Policy Based on Reinforcement Learning Markov Chain Monte Carlo Algorithm

Vahid Tavakol Aghaei<sup>1\*</sup>   Arda Ağababaoğlu<sup>2</sup>   Peiman Naseradinmousavi<sup>3</sup>  
 Sinan Yıldırım<sup>4</sup>   Serhat Yeşilyurt<sup>5</sup>   Ahmet Onat<sup>6</sup>

<sup>1</sup>Istinye University, Electrical and Electronics Engineering, Istanbul, Turkey  
 vahid.aghaei@istinye.edu.tr

<sup>2</sup>Istanbul Technical University, Arı Teknokent, Istanbul, Turkey  
 agababaoğlu@sabanciuniv.edu

<sup>3</sup>San Diego State University, Dynamic Systems and Control Laboratory, San Diego, USA  
 pnaseradinmousavi@sdsu.edu

<sup>4</sup>Sabanci University, Industrial Engineering, Istanbul, Turkey  
 sinanyildirim@sabanciuniv.edu

<sup>5</sup>Sabanci University, Mechatronics Engineering, Istanbul, Turkey  
 syesilyurt@sabanciuniv.edu

<sup>6</sup>Istanbul Technical University, Electrical and Electronics Engineering, Istanbul, Turkey  
 ahmetonat@itu.edu.tr

## Abstract

The primary focus of this paper is centered on the numerical analysis and optimal control of vertical axis wind turbines (VAWT) using Bayesian reinforcement learning (RL). We specifically tackle small-scale wind turbines with permanent magnet synchronous generator, which are well-suited to local and compact production of electrical energy in small scale such as urban and rural infrastructure installations. Through this work, we formulate and implement an RL strategy using Markov chain Monte Carlo (MCMC) algorithm to optimize the long-term energy output of the wind turbine. Our MCMC-based RL algorithm is a model-free and gradient-free algorithm, where the designer does not have to know the precise dynamics of the plant and their uncertainties. The method specifically overcomes the shortcomings typically associated with conventional solutions including but not limited to component aging, modeling errors and inaccuracies in the estimation of wind speed patterns. It has been observed to be especially successful in capturing power from wind transients; it modulates the generator load and hence rotor torque load so that the rotor tip speed reaches the optimum value for the anticipated wind speed. This ratio of rotor tip speed to wind speed is known to be critical in wind power applications. The wind to load energy efficiency of the proposed method is shown to be superior to the classical maximum power point tracking method.

## 1 Introduction

The main purpose of machine learning (ML) is to determine action policies to perform successfully in unknown environments, or tune control strategies to optimize a design goal. One of the most effective ML methodologies, also used for solving control problems, is reinforcement learning (RL) (Sutton and Barto,

---

\*Corresponding author

1998). In RL setting, an agent (controller) applies an action to achieve state transitions after which an immediate reward portraying the performance of the agent is issued. An optimal policy of selecting actions that optimize the cumulative reward is then sought. Recently, renewable energy sources have received a lot of attention as a result of increasing demands towards the ecological concerns, where wind energy conversion technologies have piqued much interest among the various renewable energy sources (Cheng and Zhu, 2014).

The most prevalent forms of wind turbines are horizontal and vertical axis ones (HAWT and VAWT) in which the rotor’s axis is either oriented horizontally or vertically with respect to the wind stream have been thoroughly investigated by Özgün Önel (2016) in terms of their merits. In parallel to the wide-spread increase in the applications of wind energy in every possible sector, the main focus of this research is the numerical analysis and optimal control of VAWTs where their operational condition is independent of wind direction. Furthermore, since they produce less noise and need less maintenance, they can be well-suited to urban and remote power generation areas, especially in small-scale applications (Khorsand et al., 2015; Tummala et al., 2016; Tasneem et al., 2020). Through this work, we formulate and implement a RL strategy using Markov Chain Monte Carlo (MCMC) algorithm to optimize the long-term energy output of the wind turbine. The method specifically overcomes the shortcomings typically associated with conventional solutions including but not limited to component aging, modeling errors and inaccuracies in the estimation of wind speed patterns. Our RL-MCMC algorithm is a model-free and gradient-free algorithm, where the designer does not have to know the precise dynamics of the plant and their uncertainties. The method has been observed to be especially successful in capturing power from wind transients; it modulates the generator load and hence rotor torque load so that the rotor tip speed reaches the optimum value for the anticipated wind speed. This ratio of rotor tip speed to wind speed is known to be critical in wind power applications. Recently, thanks to advancements in electronic and power control devices, variable-speed control (Dali et al., 2021) for wind energy conversion systems (WECSs) has enabled greater energy harvesting from the wind. Pitch angle of the rotor as well as electrical load are commonly used to regulate the speed of a WECS. Various variable-speed control algorithms such as sliding mode control (SMC) (Yang et al., 2018), MPPT (Sitharthan et al., 2020), model predictive control (MPC) (Onol et al., 2015), adaptive neuro-fuzzy (Asghar and Liu, 2018), and RL (Wei et al., 2016) have been implemented on wind turbines.

MPPT is a famous control method for VAWTs. Each turbine running at a certain wind speed has an optimal tip-speed ratio (TSR) that corresponds to a specific generator rotor speed ( $\omega_r$ ) and yields maximum power. It is this ratio and its derivative that MPPT algorithms strive to optimize. While MPPT is effective at maximizing the instantaneous power, this is not the same as maximizing the whole energy available. The three main MPPT algorithms which are elaborately addressed in Lasheen et al. (2015), are the TSR, the perturb and observe (PaO), and the power signal feedback control. Moreover, there are other MPPT methods in the literature such as hybrid-adaptive PaO (Youssef et al., 2020), fuzzy logic based MPPT with a grey-wolf optimization algorithm (Laxman et al., 2021; Seyyedabbasi and Kiani, 2021), and sensorless MPPT algorithms (Li et al., 2019). Specifically, to control the small-scale wind turbines, there exist fuzzy-based MPPT (Ngo et al., 2020; Yaakoubi et al., 2019), PaO MPPT (Syahputra and Soesanti, 2019) and limited power point tracking (LPPT) (Aourir and Locment, 2020) methods.

MPC is another typical control method utilized in the operation of VAWT. With a convex objective function and an accurate system model, this strategy can be helpful in achieving the desired results (García et al., 1989). For obtaining a wind profile-optimized control signal, this method employs a finite-horizon prediction approach. Due to the fact that MPC addresses the optimization problem using a finite-horizon, there are several circumstances in which the objective function might not be optimized as it should be. Additionally, in order to comply with MPC regulations, the future data of wind speed must be gathered and individually transmitted to the wind turbine. In cases of dramatic wind variations, MPC may not be effective due to its sluggish performance. The research that has been done on MPC for WECs has resulted in multiple different applications (Prince et al., 2021; Song et al., 2017). Despite their success, the challenge with MPC algorithms is threefold; a time horizon for control predictions must be selected, a plant model that is accurate through that horizon is required, and high computational cost is incurred for evaluating the model (Bemporad, 2015). Costs associated with MPC calculations are large, even with ML-based models. Moreover, real-time applications may not be possible depending on the control problem’s convexity and complexity (Norouzi et al., 2022).

Achieving maximum control efficiency in modern control and robotic systems is a priority, hence researchers have recently turned to ML techniques (Ouyang et al., 2022). Some researches (Bui et al., 2020; Zhang et al., 2020; Lin et al., 2021; Kofinas et al., 2017) incorporate RL into MPPT to improve

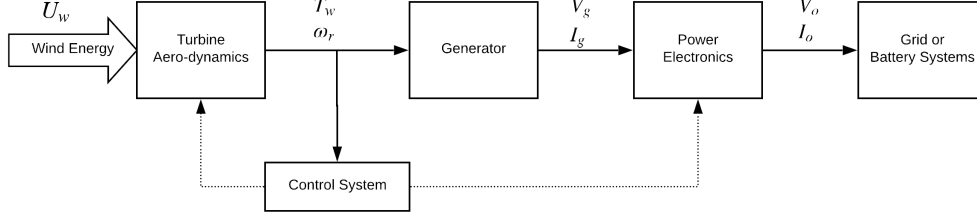


Figure 1: A Block representation of a controlled WECS.

the efficiency of MPPT; this is noteworthy given the paucity of efforts dedicated to ML-based control of WECS. Furthermore, some other works, have used artificial neural-networks to control WECS (Karthik et al., 2022; Choja et al., 2021).

To maximize the energy output in wind turbines there exist some optimal control methods (Horvat et al., 2012; Park and Law, 2015). The disadvantage of these methods are in formulating an analytical power function for a specific wind turbine model. As an alternative, a data-driven algorithm is proposed in Gebraad and van Wingerden (2015) which is based on the gradient optimization of the MPPT method. However, gradient-based algorithms may suffer from getting trapped in local optima.

When it comes to finding the optimal policy in stochastic dynamical systems, Bayesian RL has proven to be an efficient solution, especially for the control and robotics domains (Derman et al., 2020; Jia and Ma, 2021; Rana et al., 2021; Tavakol Aghaei et al., 2021). However, there is much room for improvement regarding its potential use in energy conversion systems which arouses our curiosity to contribute to filling this gap. Some of the available Bayesian methods use Gaussian processes (GP) to learn either the model of the system or the desired objective function via learning the hyper-parameters of the GPs (Brochu et al., 2010; Wilson et al., 2014). In this regard Park and Law (2016) recently applied a Bayesian method to obtain an approximate model of the target function using GPs to maximize the wind farm power. However, our method differs in that it is a model-free RL-based algorithm, which uses MCMC as a sampling strategy to draw samples from an instrumental function called *posterior distribution*. By using the *Bayes' theorem* we construct the posterior distribution, which is proportional to the objective function of the RL algorithm and some *prior* density functions of the unknown parameters of the RBFNN controller. It is shown that the drawn samples from this posterior function will ultimately converge to the exact target function (Andrieu et al., 2003). One disadvantage of the proposed Bayesian algorithm by Park and Law (2016) is the computational cost of the GP regression model, whereas this issue is tackled in our proposed RL-MCMC method since we do not model the cost function and instead we build a posterior function which we can draw samples from and is guaranteed to converge to the desired target function. Another disadvantage with their method is the problems related to the *trust-region* optimization method which they impose some constraints over the parameter search space. This results in finding local optimal solutions that are close to their initial parameters. Unlike their method, and inspired by the *exploration-exploitation* problem, we have developed an RL-MCMC algorithm that benefits from the strengths of both the gradient-free Bayesian MCMC and RL algorithms. We use MCMC sampling method that is capable of exploring the *high-reward* regions of the policy parameter space (benefiting from the long-term rewards in RL). Since the policy space is explored in a non-contiguous manner, different regions can be visited and the probability of discovering better performing regions always exists. The main point is that, our proposed Algorithm 1 is not designed to converge to a single point. Instead, the policy parameters are guaranteed to follow the probability distribution  $\pi(\theta)$  stated in Equation (16). In terms of being a *gradient-free* algorithm, there already exists some algorithms to analytically evaluate a target function (Powell, 2008; Chang et al., 2013; Rios and Sahinidis, 2013). However, in our case, the objective function given in Equation (14) is not analytically known. As a result we propose to use another alternative as the MCMC sampling method. Moreover, for the above-mentioned algorithms, a *trust-region* is defined as a constraint over the search space which may guide the optimization towards local optima. It should also be noted that our Bayesian RL-MCMC algorithm has the advantage of being independent of the aerodynamic model of the system, considering the fact that a model-based control has weaknesses about the fluctuations in wind turbine parameters given that the power production is dependent on a variety of factors (Soleimanzadeh and Wisniewski, 2011).

The optimization of the output energy of WECS is one of the most challenging issues to be addressed. Generally speaking, the classic control methods for wind turbine systems are not designed with long term

optimization in-mind. It is important to devise an online smart optimization strategy that will enable an efficient control mechanism to be applied in the case of fluctuating wind patterns. Additionally, it is important to note that not every algorithm is optimal for systems which are linearized. Therefore, standard wind conversion systems face persistent difficulties in adapting to changing wind conditions. Our proposal is to use a hybrid artificial intelligence and ML-based methodology that account for nonlinearities and uncertainties to address these challenges. At the heart of the control policy, a nonlinear RBFNN controller is developed in which its unknown parameters are being learned by an RL-MCMC method proposed in Aghaei et al. (2018). In the current paper however, we reshaped that original method and improved it through the inclusion of RBFNN as a nonlinear controller that will enable us to learn to control the unknown WAWT system. Similar to our control structure, recently, Keighobadi et al. (2022) used a SMC with an RBFNN to compensate for the uncertainties and noises involved in the control of the wind turbines. However for our case, RBFNN is used as a neural control policy and we incorporate the system uncertainties into the long-term reward function of the RL algorithm,  $J(\theta)$ . Based on a known load current and voltage ( $I_L$ ,  $V_L$ ), rotor speed  $\omega_r$ , wind speed  $U_w$  and its derivative, the proposed algorithm is capable of learning to control the VAWT's unknown model and can obtain the immediate control effort  $I_L$  similar to the optimal load coefficient  $C_L$ . It also facilitates recognizing different variations (as friction, tear and wear of the blades, and elements aging) in VAWT dynamics over time.

Our focus is on a small-scale VAWT with a 3-bladed rotor structure. Comparing MPPT with the proposed RL-MCMC algorithm, demonstrated the efficiency of the proposed method. Furthermore, its performance in terms of convergence has been shown.

The contributions of the current paper, inspired by the need for novel configurations for the renewable energy systems capable of optimizing the output energy, can be summarized as follows:

#### 1. ML-based control of turbine and its responses to wind patterns

- (a) To learn to control VAWT's unknown dynamics, the proposed control structure employs a nonlinear RBFNN controller (calculating the reference load current  $I_{L_{ref}}$ ), which its unknown parameters are learned using RL-MCMC.
- (b) The proposed control methodology can learn to respond to arbitrary and unpredictable wind profiles.
- (c) Provides a way of continuously adapting the controller to the changing wind patterns which makes it possible to the designer to install the VAWT in any location and still obtain the maximum available energy from the wind.

#### 2. Developing a Bayesian gradient-free and model-free algorithm

- (a) Shape of the objective function in Equation (14) is not explicitly known. Therefore, gradient and Hessian approximations cannot be a suitable choice for analytical solutions. In the considered setting, function evaluations by various simulations are costly. Thus, by leveraging MCMC, we could guide the search mechanism to the regions where obtaining the optimal parameters are most likely (high-reward areas).
- (b) Developing a model-free algorithm which operates regardless of the aerodynamics model of system.

#### 3. Comprehensive simulation studies and comparisons with MPPT algorithm

- (a) Maximize total energy output rather than existing greedy algorithms which typically aim to maximize instantaneous output power.
- (b) Based on three different simulation scenarios, we demonstrate that the proposed RL-MCMC algorithm with an RBFNN controller outperforms the well-known classical MPPT.

In particular, our MCMC-based RL algorithm is a model-free and gradient-free algorithm, where the designer does not have to know the precise dynamics of the plant and their uncertainties. We formulate the overall effect of such uncertainties into an expected total reward  $J(\theta)$ , which is given in Equation (14). It maximizes  $J(\theta)$  of an instantaneous reward function ( $r(t)$ ) created by the designer, and calculates an action policy  $\pi_\theta$ , where  $\theta$  is the set of controller parameters. We can take, for example, the instantaneous electrical output power as part of the reward function and our RL-MCMC algorithm maximizes its cumulative value, e.g., total energy output. To explore policies according to  $J(\theta)$ , the algorithm does not have to evaluate  $J(\theta)$  explicitly; but by merely approximating it via MCMC. This is in fact one of the advantages of our methodology which we stress throughout the manuscript.

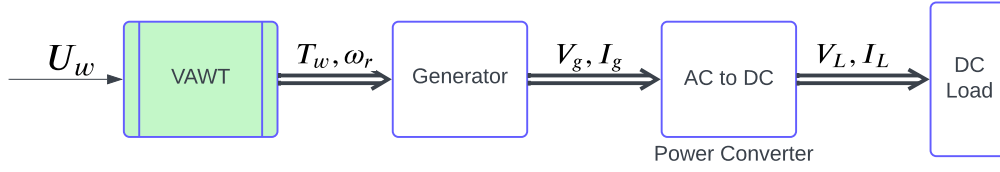


Figure 2: A schematic representation of the system

Table 1: Parametrization of the system model.

Description	Symbol	Quantity	
Rotor inertia	$J_r$	2	$kg.m^2$
Rotor radius	$r_r$	0.5	$m$
Blade length	$l_b$	1	$m$
Friction coefficient	$b_{fr}$	0.02	$Ns/rad$
Air density	$\rho$	1.2	$kg/m^3$

## 2 VAWT Model

The VAWT's aerodynamics, the power-electronic structure, the load and generator models are all discussed in detail in this part. This paper uses the model and settings presented in Sancar (2015) to simulate the VAWT system. The block diagram representations, for the VAWT system and the control approach for WECS, are illustrated in Figures 1 (Ağababaoğlu, 2019) and 2.

Wind turbines use aerodynamics to transform the kinetic energy of the wind into mechanical energy, providing torque for a generator at a rotational speed  $\omega_r$  and torque  $T_w$ . In this setup, a wind-powered generator produces electricity. The control mechanism typically measures  $\omega_r$  and  $T_w$  to derive reference load current as the required control effort. The amount of generated power depends on the wind's velocity  $U_w$  and rotor's aerodynamics ( $\rho C_p S_a$  representing density of air, wind power coefficient, and wind turbine's swept area using rotor radius  $r_r$  and length of blade  $l_b$ ) according to equation (1) (Da Rosa and Ordóñez, 2021).

$$\mathcal{P} = 0.5\rho C_p S_a U_w^3 \quad \text{with} \quad S_a = 2r_r l_b \quad (1)$$

The conversion of the wind energy is limited by the aerodynamic efficiency of the rotor  $C_p$ . For a given wind speed, there is a rotor speed  $\omega_r$  such that the TSR is at the maximum of the  $C_p$  curve. This operating point ensures maximum aerodynamic efficiency, which is the main objective of most studies devoted to improving the energy efficiency of wind turbines.

### 2.1 VAWT Parameters and Mathematical Model

It should also be noted that  $C_p$  itself is a function of TSR ( $\lambda$ ) that is given in equation (2):

$$\lambda = \frac{\omega_r r_r}{U_w} \quad (2)$$

In order to simulate the behaviour of the wind and VAWT, equation (3), which is the extension of equation (2), is used. These equations give the maximum possible value for  $C_p$  as around 0.4, as also seen from Figure 3. For our setting, the VAWT parameter values are provided in Table 1. Besides these structural parameters, a 6<sup>th</sup> order nonlinear relationship between  $C_p$  and TSR is experimentally established as given in equation (4a).

$$\mathcal{P} = \rho C_p(\lambda) r_r l_b U_w^3 \quad (3)$$

$$C_p(\lambda) = p_1 \lambda^6 + p_2 \lambda^5 + p_3 \lambda^4 + p_4 \lambda^3 + p_5 \lambda^2 + p_6 \lambda \quad (4a)$$

$$p_i = [-0.3015, 1.9004, -4.3520, 4.1121, -1.2969, 0.2954] \quad \text{for} \quad i = 1, \dots, 6 \quad (4b)$$

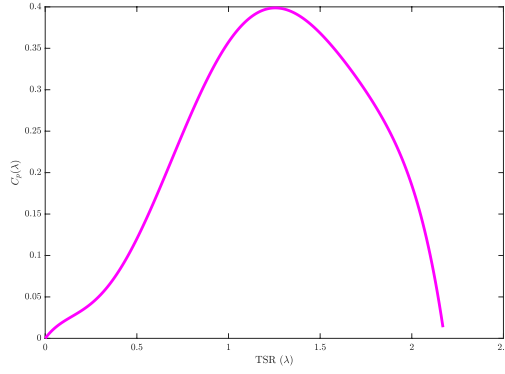


Figure 3:  $\lambda - C_p$  curve of studied system

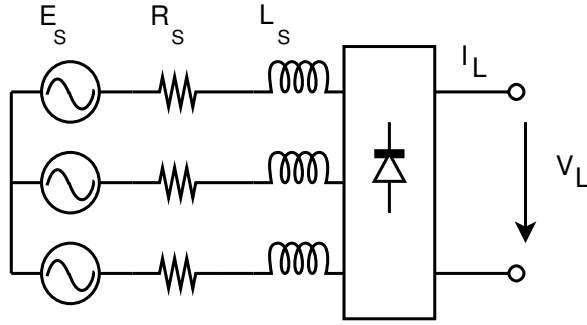


Figure 4: Three-phase PMSG-Rectifier schematic.

Equation (4b) provides different  $C_p$  values and in Figure 3 a curve representing  $C_p$  with respect to  $\lambda$  has been shown. One can also obtain generated torque by the wind by having the ratio between wind power and rotor velocity as in equation (5).

$$T_w = \frac{P_w}{\omega_r} = \frac{\rho C_p(\lambda) r_r l_b U_w^3}{\omega_r} \quad (5)$$

## 2.2 Three-Phase PMSG-Rectifier's Model in the VAWT Structure

Dynamical equation for the rotor's PMSG can be written as equation (6) according to Tripathi et al. (2015) where  $T_g$  and  $T_{fr}$  are generator and friction torques (equations (7)-(8)), respectively.

$$J_r \frac{d\omega_r}{dt} + T_{fr} + T_g - T_w = 0 \quad (6)$$

$$T_g = \mathcal{K}_t I_L \quad (7)$$

$$T_{fr} = b_{fr} \omega_r \quad (8)$$

Figure 4 is an illustration of the PMSG-rectifier circuit. In this figure,  $L_s$ ,  $R_s$ , and  $E_s$  represent inductance, resistance and electromotive force for the PMSG, respectively.

Load voltage  $V_L$ , can be calculated as shown by equation (9), taking into account both the load current  $I_L$  and  $\omega_r$  in which a zero  $I_L$  will bring the  $V_L$  to its highest value. Because of the presence of  $T_g$ , the more one increases  $I_L$ , the more decrease will occur for  $V_L$ , as well.

$$V_L = \sqrt{E_{SDC}^2 + (p\omega_r L_{dc} I_L)^2} - (R_{dc} + R_D) I_L \quad (9)$$

Figures 4 and 5 illustrate, respectively, the PMSG-rectifier model and its corresponding DC circuit, where their parameters can be specified according to Table 2. The PMSG-Rectifier voltage drops are due to both  $R_{dc}$  and  $R_D$  (equation (10)) resistors, where the latter is used to design a more practical

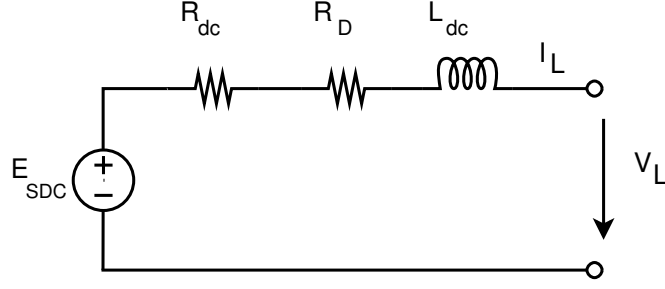


Figure 5: PMSG-Rectifier's modified DC model.

Table 2: PMSG-Rectifier parameters.

Description	Equivalent PMSG	Simplified DC Model
Flux	$\phi_s$	$\phi_{dc} = 3\sqrt{6}\phi_s/\pi$
EMF	$E_s = \phi_s p \omega_r$	$E_{SDC} = 3\sqrt{6}E_s/\pi$
Inductance	$L_s$	$L_{dc} = 18L_s/\pi^2$
Resistance	$R_s$	$R_{dc} = 18R_s/\pi^2$

DC structure based upon the mean of the voltage drops associated with the generator's rotor reaction, commutating and overlapped currents in the three-phase diode bridge.

$$R_D = \frac{3L_s p \omega_r}{\pi} \quad (10)$$

### 2.3 The Load Model of VAWT

In this study a simplified load circuit consisting of a variable load resistor is used as depicted in Figure 6. Adjusting  $R_L$  to increase  $I_L$ , will produce a large load-torque to the turbine mechanics; alternatively, decreasing  $I_L$ , will likewise decrease the generator torque. The RL-MCMC algorithm is thus responsible for regulating  $I_L$  so that the  $\omega_r$  may be adjusted in order to achieve the highest possible output energy.

## 3 Structure of the RL and MCMC

As the controller (agent) in the RL setting iteratively via a decision-making process interacts with the environment in which they operate, the system may learn the optimal policy behavior. It is through the selection of actions that an agent may gain knowledge from the experiences it has had. The agent gets an observation for per step  $t$ , executes an action and moves to a new state in its environment, and is rewarded with a real-valued number  $r_t \in \mathbb{R}$ ; in the long run, RL seeks to discover a policy that maximizes this value. The policy may be thought of as a function that connects observations with the appropriate actions. The main components of an RL problem can be formulized using the following set:

$$(S, A, \xi, \vartheta, r)$$

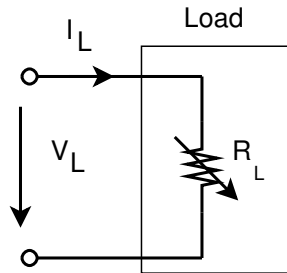


Figure 6: Load controlled by optimization algorithm

For representing set of continuous state and action spaces separately, we use  $S$  and  $A$  where each individual state-action for a given time step  $t$  belongs to these spaces. For each  $t$ , the agent's future state  $s_{t+1}$  is determined by a transition dynamic distribution  $\xi(\cdot)$  having the present state-action of the agent  $(s_t, a_t)$ , where  $\vartheta(\cdot)$  is the initial state function.

$$\xi(s_{t+1}|s_t, a_t) \quad \forall s, s_{t+1} \in S, \quad \forall a_t \in A$$

The policy is indicated by a parameterized ( $\theta \in \mathbb{R}^{d_\theta}$ ) distribution  $h_\theta(a_t|s_t)$  where they can be chosen from a stochastic *Gaussian* density, allowing for a proactive exploration of the state-space. Assuming  $X_t = (S_t, A_t)$ , forms a Markov chain state-action trajectory for  $\{X_t\}_{t \geq 1}$  with a transition law given in (11) where state-action pair for time  $t$  is defined as  $x_t = (s_t, a_t)$ .

$$f_\theta(x_{t+1}|x_t) := \xi(s_{t+1}|s_t, a_t)h_\theta(a_t|s_t). \quad (11)$$

To have a measure of the the conformity of the state transitions for a whole trajectory, weighted rewards' summation ( $\gamma \in (0, 1]$ ) over a time  $T$  is calculated; namely called *return*

$$R(x_{1:T}) = \sum_{t=1}^T \gamma^{t-1} r_t. \quad (12)$$

Moreover, the joint distribution of the trajectory  $x_{1:T}$  can be given as,

$$p_\theta(x_{1:T}) = \vartheta(s_1) \prod_{t=1}^T f_\theta(x_{t+1}|x_t) \quad (13)$$

with  $\vartheta(s_1)$  implying an initial state distribution in which  $s_1 \sim \vartheta(\cdot)$ . Having the trajectories' distribution and return, a cost function  $J(\theta)$ , evaluating the police's performance, can be defined,

$$J(\theta) = \mathbb{E}_\theta[R(x_{1:T})] = \int p_\theta(x_{1:T}) R(x_{1:T}) dx_{1:T}. \quad (14)$$

In RL, optimizing policy is its main purpose to finding ideal parameters  $\theta^*$ . This could be accomplished by maximizing the return expectations over a trajectory:

$$\theta^* = \arg \max_{\theta \in \Theta} J(\theta) \quad (15)$$

It is important to recognize that the trajectory's density in (13) might be complicated or even partially known. Thus for such a density function, the integral must be addressed in equation (14), which is numerically insoluble. Levine et al. (2016); Durrant-Whyte et al. (2012); Peters and Schaal (2008) have come up with several cutting-edge gradient-based RL algorithms in order to cope with this issue. However, one major challenge with the gradient-based methods is the local optimal solution. Opposed to these methods, Bayesian approaches are used to explore the possible high reward areas of the parameter space  $\Theta$  in seeking optimal policy parameters as shown in Pautrat et al. (2018); Marco et al. (2017); Gal and Ghahramani (2016). Inspired by the *exploration-exploitation* dilemma in RL, problems related to the gradient-based RL, and based on the existing gap in applying Bayesian optimization methods in WECS, we provide an RL-based Bayesian method with an RBFNN controller which is capable of being applied to energy systems.

### 3.1 RL-MCMC applied to the Dynamical Systems

The suggested method, which is applicable to systems with continuous domains, is an MCMC-based policy search algorithm based on RL to control the WECS.

In comparison to gradient-based RL, the Bayesian-MCMC offers a number of significant benefits. Its mathematical simplicity, along with the fact that it is not reliant on gradient computations, enables it to avoid being mired in locally optimal solutions.

Since the calculation of  $J(\theta)$ , entails prohibitive computational effort, we propose forming a density function that includes the policy parameters' prior distributions  $\mu(\theta)$ . Then, assuming the Markovian ergodicity property of parameters, the constructed density function, aka *posterior*, is sampled by the MCMC algorithm, where expectation calculations are hard to achieve

$$\pi(\theta) \propto \mu(\theta)J(\theta) \quad (16)$$



In MCMC, the target distribution is created accepting two properties of the chain as *invariance* and *ergodicity*, which is being initialized with a given  $\theta^{(0)}$ . As an MCMC algorithm, Metropolis-Hastings (MH) selects the appropriate candidate parameter from a distribution of proposals i.e.  $\theta^\dagger \sim \Gamma(\theta^\dagger|\theta)$ . The suggested sample is then either taken with an acceptability degree given in (17), in which case the value of the current parameter is substituted with the new one, or dismissed, in which case the current parameter remains unchanged.

$$\varrho(\theta, \theta^\dagger) = \frac{\Gamma(\theta|\theta^\dagger) \mu(\theta^\dagger) J(\theta^\dagger)}{\Gamma(\theta^\dagger|\theta) \mu(\theta) J(\theta)} \quad (17)$$

An analytical calculation appears to be impossible due to the presence of  $J(\theta)$  and  $J(\theta^\dagger)$  in (17). However, an estimator with the property of obtaining unbiased and non-negative approximations of  $J(\theta)$ , enables us to sample from  $\pi(\theta)$ . This is generally possible by using an importance sampling (IS) problem. For WECS, the proposed learning algorithm is given in Algorithm 1.

---

**Algorithm 1** RL-MCMC learning mechanism for WECS

---

**Input:** Initialize policy parameters and estimated cost ( $\theta^{(0)} = [\sigma^{(0)} \quad w^{(0)}], J^{(0)}$ )

**Output:** Policy parameters  $\theta^{(\ell)}$ ,  $\ell = 1, 2, \dots$

**for**  $\ell = 1, 2, \dots$  **do**

    sample a candidate parameter  $\theta^\dagger \sim \Gamma(\theta^\dagger|\theta)$ .

    Simulate WECS by proposed parameter  $\theta^\dagger$  and calculate the state-action  $x_t = (s_t, a_t) = (\dot{e}, I_{L_{ref}})$

    Calculate the reward  $r_t = -s_t^2 Q$

    Cost estimation using standard IS:  $J(\theta^\dagger) = (\sum_{t=1}^T r_t)$

    Choose candidate by a probability of  $\min\{\varrho(\theta, \theta^\dagger), 1\}$ , put  $\theta^{(\ell)} = \theta^\dagger$  and  $J^{(\ell)} = J^\dagger$

$$\varrho(\theta, \theta^\dagger) = \frac{\Gamma(\theta|\theta^\dagger) \mu(\theta^\dagger) J^\dagger}{\Gamma(\theta^\dagger|\theta) \mu(\theta) J},$$

    else candidate is rejected,  $\theta^{(\ell)} = \theta$  and  $J^{(\ell)} = J$ .

**end**

---

## 4 Proposed Control Structure

Our goal is to create a framework that along with the ability to control VAWT's system with unknown dynamics can also obtain desirable responses towards different wind velocity profiles. In the present part, we will cover the RL environment, the RBFNN controller architecture, and different steps to train the proposed RL- MCMC algorithm for the WAVT. To improve the overall electrical energy output of the WAVT system, the instantaneous current of the load  $I_L$  in the generator will be optimized provided that the current and voltage in the load do not exceed their maximum values. For this purpose, an RBFNN controller is used to compute the corresponding current in the load as a reference  $I_{L_{ref}}$ , where the proposed control structure can be feasible for the RL-MCMC algorithm in learning the unknown parameters of the VAWT.

The instantaneous electrical power can be integrated within a given interval, to determine the desired energy output using the formula (18). The ideal aerodynamic power is produced by the rotor upon continually keeping  $C_p$  at its highest amount, and integrating over it yields the maximum reference mechanical energy, which is then converted to an optimal electrical energy value (Sancar, 2015) which results in (19). After calculating  $E_{out}$  and  $E^*$ , the resulting energy error, which its derivative will be used as the required state of the learning algorithm, can simply be obtained as (20).

$$E_{out} = \int_0^\tau P dt \quad (18)$$

$$E^* = \int_0^\tau P^* dt \quad (19)$$

$$e = E^* - E \quad (20)$$

Similar to the state of the learning algorithm  $\dot{e}$ , a continuous action  $I_{L_{ref}}$  with a single dimension is considered.

Table 3: RBFNN structure and its parameters

Inputs for the RBFNN	Structural parameters	Parameter description
$x_1$	$U_w$	Wind Speed
$x_2$	$\dot{U}_w$	Wind speed derivative
$x_3$	$I_L$	Current for the load
$x_4$	$V_L$	Voltage for the load
$x_5$	$\omega_r$	Rotational velocity for PMSG
$x_6$	$\dot{\omega}_r$	PMSG Rotational velocity's derivative

#### 4.1 RBFNN as the Controller

A nonlinear RBFNN control given in (21) is designed to calculate the reference load current  $I_{L_{ref}}$  with  $n$  hidden nodes.

$$F(x, \theta) = \sum_{i=1}^n w_i \mathcal{R}_i(x) + b \quad (21)$$

where,  $\theta$  shows the adjustable parameters of the system:  $\theta = [w \ \sigma]$ .

The Gaussian receptive field  $\mathcal{R}_i(x)$  with input  $x$  as shown in Table 3 is defined in (22) (with centers  $c_{ij}$  and variance  $\sigma_j^2$ ), calculates  $i^{th}$  node output,  $b$  is a biasing scalar value, and  $w_i$ s represent the weights.

$$\mathcal{R}_i(x) = \sum_{j=1}^m \exp\left(-\frac{\|(x_j - c_{ij})\|^2}{2\sigma_j^2}\right) \quad (22)$$

$$c_{ij} = \begin{bmatrix} c_{11} & \dots & c_{1m} \\ \vdots & \ddots & \vdots \\ c_{n1} & \dots & c_{nm} \end{bmatrix} \quad (23a)$$

$$\sigma = [\sigma_1 \ \sigma_2 \ \dots \ \sigma_m]^T \quad (23b)$$

In our model,  $c_{ij}$  matrix is defined by taking the relevant interval of related variable and dividing them into 5 equally spaced intervals, each of which contains an RBF function. Table 4 lists the boundary points of the intervals where they are selected according to the working region of the inputs of RBFNN. The inputs for the RBFNN are given as in Table 3 which is arranged taking into account the probable wind profiles as well as the internal dynamics of the VAWT. In this regard, the physical parameter  $U_w$  and its derivative  $\dot{U}_w$ , are chosen as the primary means through which wind velocity and its rate of change may be perceived by RBFNN. On the other hand, VAWT's internal states such as a  $V_L$ ,  $I_L$ ,  $\omega_r$ , and  $\dot{\omega}_r$  are fed into the neural controller.

The proposed RL-MCMC approach is implemented to learn  $\theta$  parameters of the controller. Taking advantage of such compound learning mechanism, an improved performance, when experiencing real winds, will be achieved via determining the ideal  $I_{L_{ref}}$  for all possible windy situations. Moreover, it can help to learn an unknown model of the system by characterizing and encoding the model parameters into RBFNN structure. Refer to the diagram in figure 7 to see how the suggested control mechanism is performing.

#### 4.2 Training Procedure of the Learning Algorithm

The section explains the way that the control parameters could be taught under intricate wind samples. The training is begun by applying three different wind profiles as step, sinusoidal and realistic wind data with an initial parameter set  $\theta_{S0}$  to learn the optimal parameter sets  $\theta_{S1}$ ,  $\theta_{S2}$ . The training scheme is carried out as follow:

- **Step 1:** The parameters for the policy are initialized as  $\theta_{S0}$
- **Step 2:** In the first stage of training, a step wind signal is applied to the VAWT and  $\theta_{S1}$  is learned.
- **Step 3:** During training's  $2^{nd}$  stage, a sine wind signal is applied to the VAWT and  $\theta_{S2}$  is obtained.

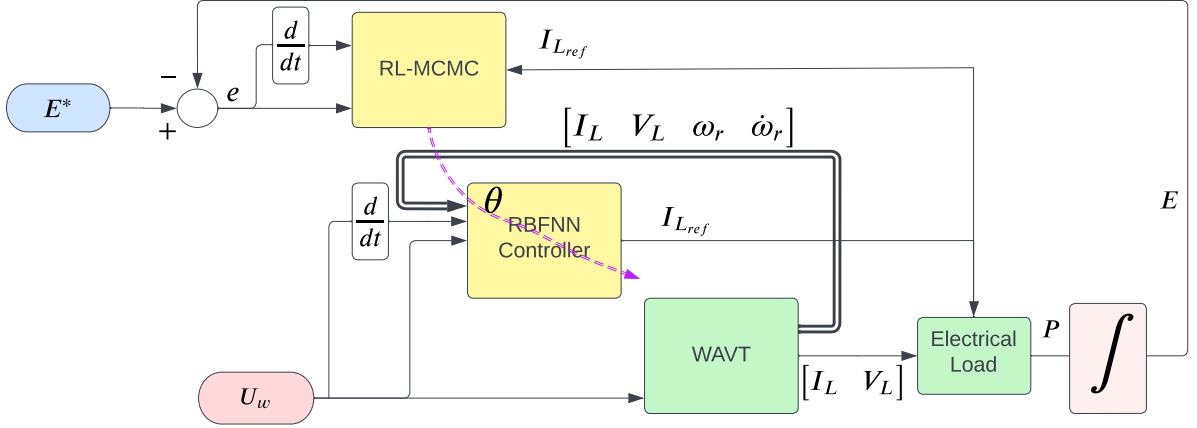


Figure 7: RL–MCMC learning block diagram for WAVT with the proposed RBFNN controller.

The reason for selecting a step wind is to consider it as a simple signal which enables the rotor for an energy management strategy. Afterwards, training’s 2<sup>nd</sup> stage targets to learn a controller to be responsive to a wind profile with changing speed. Therefore, a sinusoidal wind with a close frequency to that of the realistic ones, is selected. In an actual use case, the system would be presented to the customer having completed up to Step 3 training, where it is partially but not completely optimized. After commissioning, the system adapts to the local wind patterns. Without initial training up to Step 3, convergence to the best pattern can be impossible for the system within a reasonable time.

## 5 Outcomes from Simulated Experiments and Discussions

To demonstrate the efficiency of the proposed RL-MCMC algorithm over the classical MPPT method, an extensive simulation procedure is done for two different MPPT structures as shown in Table 6. In the first part of this section, numerical values for the parameters of the RL-MCMC structure and the RBFNN controller used in this section are given. In the second part, the results of each step of training as detailed in Sec. 4.2 of the proposed method are given. After parameter initialization in Step 1, a step wind is implemented into the system in Step 2 and the learned policy parameters during training stages of the RL-MCMC and the resulting time response specifications of the VAWT ( $P, \omega_r, V_L, I_L$ , and  $R_L$ ) are illustrated. In Step 3, a sinusoidal wind is applied and their corresponding time responses and learned parameters are provided. Finally, in Step 4, for a better comparison, a realistic wind profile with noise is applied to the system.

### 5.1 Numerical values of RL-MCMC for Simulations

For the proposed RL-MCMC algorithm the reward function is taken as,

$$r_t = -s_t^2 Q \quad (24)$$

with a state weight  $Q = 10^5$  and state  $s_t = \dot{e}$ . We assume an average return function with  $\gamma = 1$  in (12).

Policy parameters in the RL-MCMC, are updated according to a Gaussian random walk with a proposal density as  $\Gamma(\theta^\dagger | \theta) = \mathcal{N}(\theta^\dagger; \theta, \Sigma_\Gamma)$  in which a covariance matrix  $\Sigma_\Gamma$  is defined as  $\text{diag} \left( \begin{bmatrix} 1 & \dots & 1 \end{bmatrix}_{1 \times \dim(\theta)} \right)$ .

The prior distribution  $\mu(\theta)$ , for policy is  $\mathcal{N} \left( 0; \text{diag} \left( \begin{bmatrix} 10^4 & \dots & 10^4 \end{bmatrix}_{1 \times n_\theta}^T \right), \Sigma_\Gamma \right)$ , where  $\dim(\theta) = 12$  is the total number of parameters to be learned. The sampling time of VAWT dynamics is 1 ms. Also, RBFNN structure is shown in Table 4 with a bias value as 3.5.

### 5.2 RL–MCMC’s 1<sup>st</sup> Training Stage

Since the examined VAWT’s working region for  $U_w$  belongs to  $[6, 12] \frac{m}{s}$ , a wind as a step function of  $8 \frac{m}{s}$  amplitude is applied. To obtain VAWT’s dynamic performance, simulation time is selected as 150 s.

Table 4: Ranges of RBFNN Inputs.

RBFNN Input	Symbol	Min Center	Max Center
$x_1$	$U_w$	4.66	11.31
$x_2$	$\dot{U}_w$	-8.33	8.32
$x_3$	$I_L$	0.83	9.13
$x_4$	$V_L$	3.32	36.52
$x_5$	$\omega_r$	5	35
$x_6$	$\dot{\omega}_r$	-4.998	4.992

The vector of initial parameters  $\theta_{S0}$  is defined as:

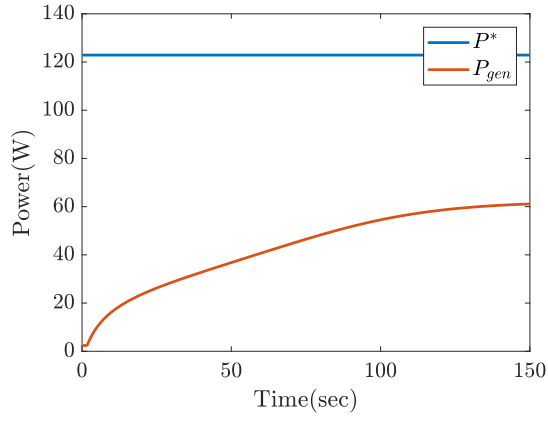
$$\theta_{S0} = [\sigma_{S0} \quad w_{S0}]$$

where for  $\sigma_{S0}$  and  $w_{S0}$  we have  $\frac{n_\theta}{2}$  parameters in which for each of them  $\sigma_{S0} = 20$  and  $w_{S0} = 1$

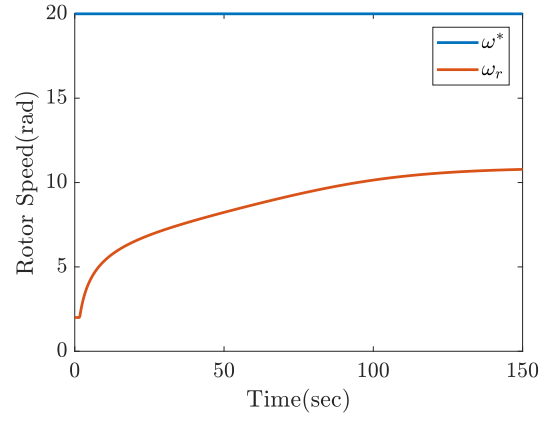
The response of the system before learning takes place using  $\theta_{S0}$ , is illustrated in Figure 8. As can be seen, the system has inferior performance as expected. Figure 8 is displayed here only as a baseline.

The evolution of policy parameters and their corresponding return during the first stage of training are shown in Figure 9a, 9b, and 9c, respectively. The learning has to be terminated early to prevent over-fitting, at  $200^{th}$  iteration. The first-stage training parameters ( $\theta_{S1}$ ) are generated by taking the average of sample parameters after the parameters have achieved a stable distribution. In our case the average value of each parameter in the last 50 iterations is taken as its final value.

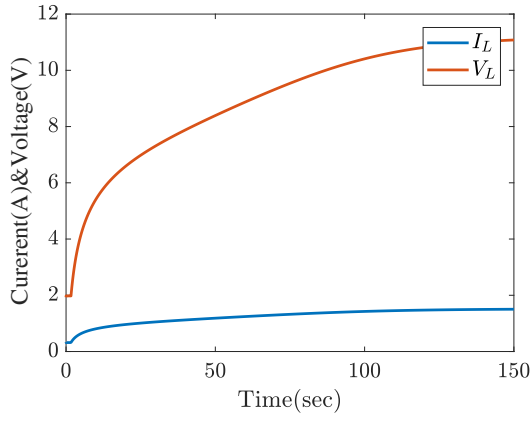
The time response is a more intuitive result, and is shown in Figure 10. The performance of the system has improved compared to the parameter set  $\theta_{S0}$  and it can effectively deal with the applied wind. However, the performance is still far from optimal due to richness in the training set.



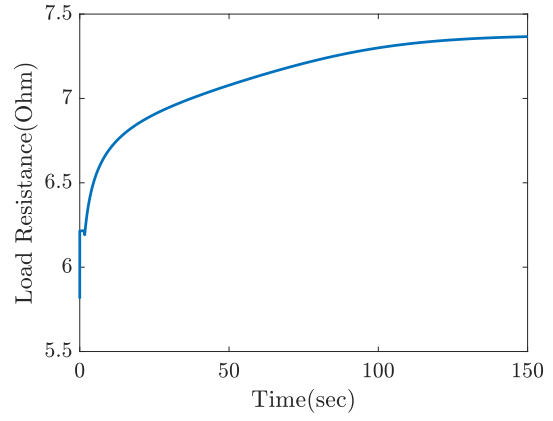
(a) Nominal versus obtained power.



(b) Rotor's angular velocity.

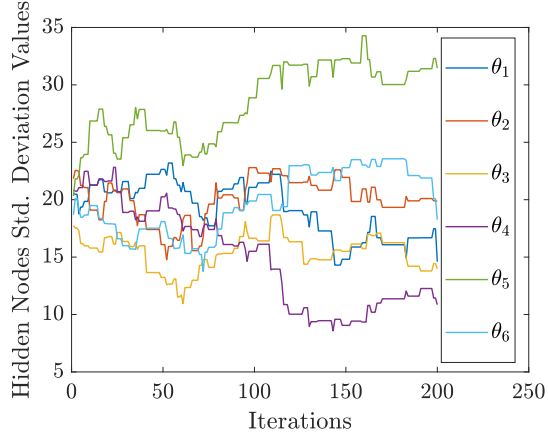


(c) Measured current and voltage in the load.

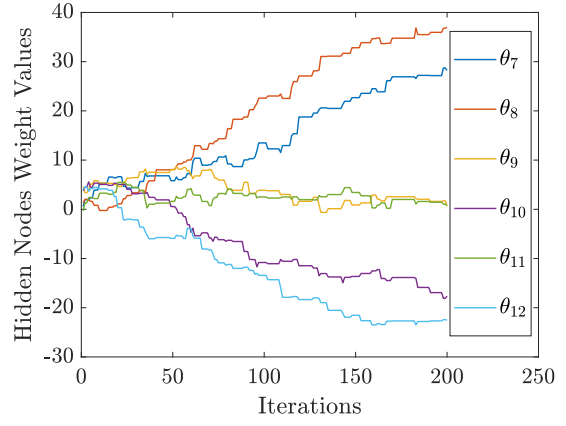


(d) Resistance of the load.

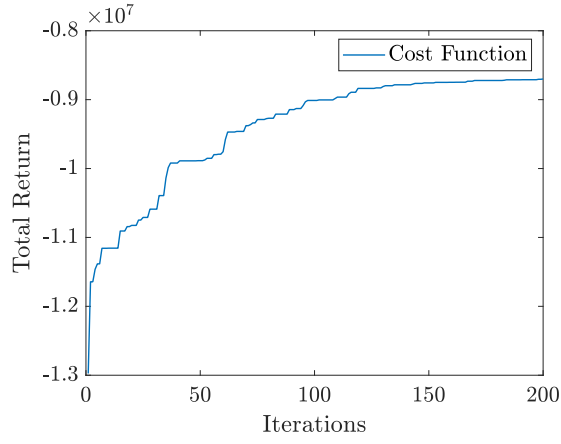
Figure 8: Time response results for  $P$ ,  $\omega_r$ ,  $V_L$ ,  $I_L$ , and  $R_L$  by RL-MCMC using initial parameters  $\theta_{S0}$ .



(a) Learned standard deviation.

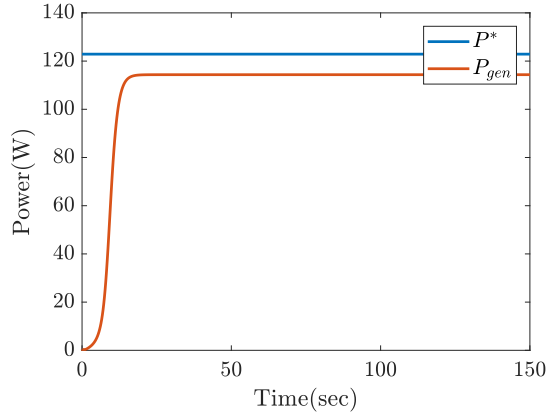


(b) Learned weights.

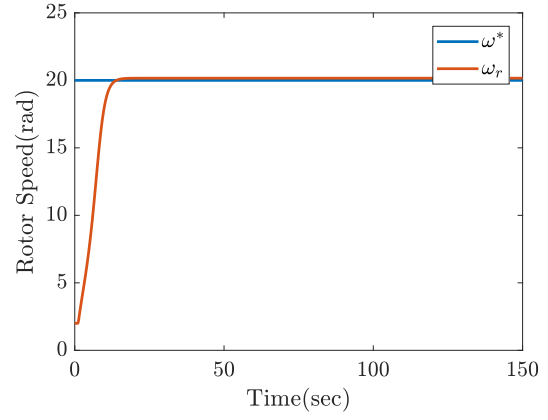


(c) Convergence plot considering return.

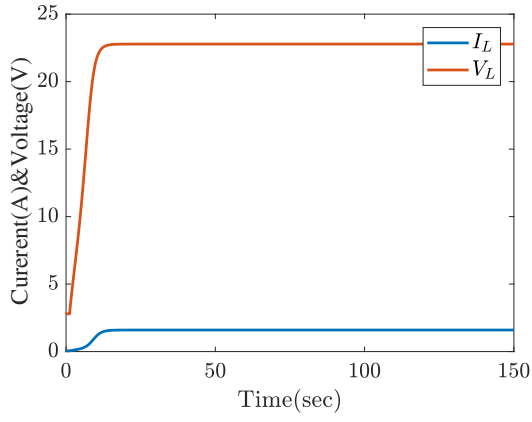
Figure 9: Trace plots of the parameters and the return during the first stage of training.



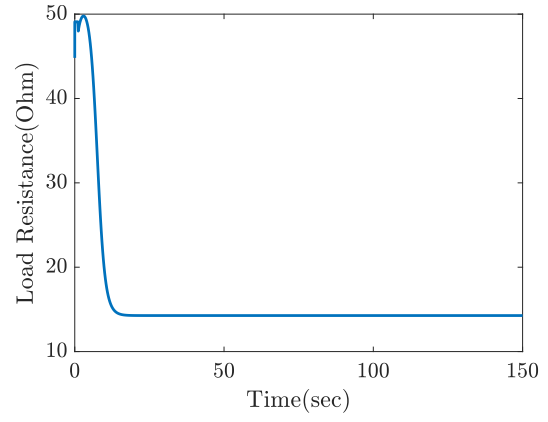
(a) Nominal versus obtained power



(b) Rotor's angular velocity



(c) Measured current and voltage in the load



(d) Resistance of the load

Figure 10: Time response results for  $P$ ,  $\omega_r$ ,  $V_L$ ,  $I_L$  and  $R_L$  by RL-MCMC after first stage training, using  $\theta_{S1}$  parameters.

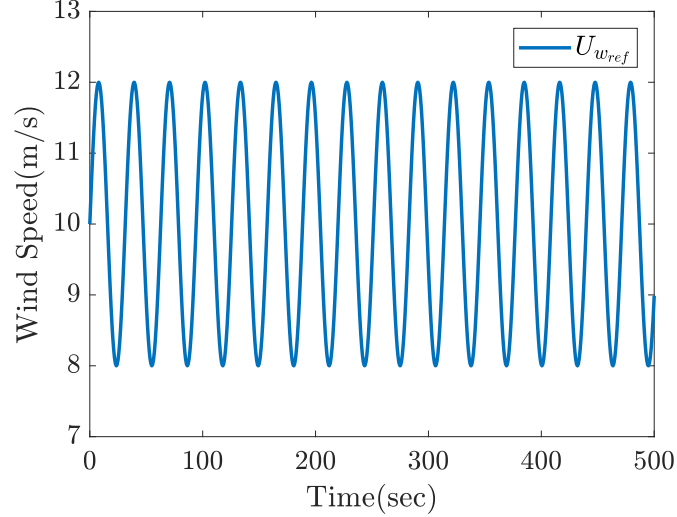


Figure 11: The wind speed reference during the second stage.

The resultant RL-MCMC controller produces a rotor speed for the generator that is close to the optimal value, as shown in Figure 10b. More importantly the proposed control algorithm does not exhibit the type of harsh rise for the current as seen in Figure 10c, but instead there is a delay before the current increases. This delay is important because it allows a light load on the rotor, allowing it to accelerate to optimum speed  $\omega_r$  quickly. In e.g. an MPPT controller, a step wind would produce an immediate rise in the current which is a greedy approach that maximizes instantaneous power but delays the acceleration of the rotor to the optimal speed due to increased mechanical load, and thus reduces the total energy output of the system.

### 5.3 RL-MCMC's 2<sup>nd</sup> Training Stage

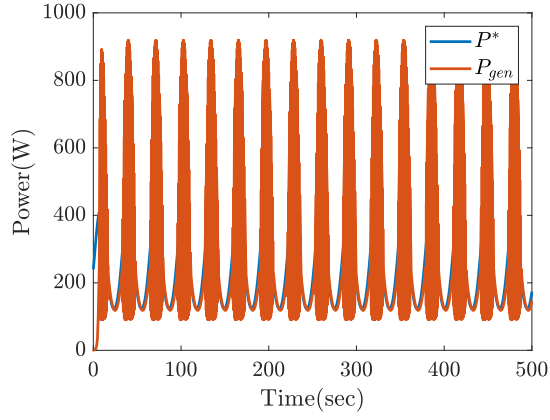
The subsequent training stage is designed to present a richer experience to obtain a control strategy capable of handling wind speeds that exhibit constant variations. In order to accomplish this, the wind,  $U_{wref}$ , is taken as a sine wave, which can be observed in Figure 11, and defined as follows:

$$U_{wref} = 10 + 2\sin(0.2t) \quad (25)$$

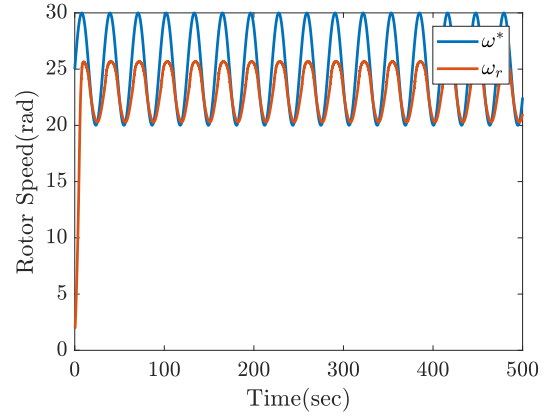
For the second phase of training, we use parameter set  $\theta_{S1}$  from the result of the first training phase as our initial parameter set. Figure 12 shows generator's performance with  $\theta_{S1}$  under a sine wave wind pattern (before second stage learning), and will be used to compare the proposed methodology's performance using  $\theta_{S2}$ , which will be obtained after second stage training is completed. From Figure 12d, load resistance can be seen to experience noisy peaks leading to the same peak profiles for both generated power and load voltage. First stage training has not provided any opportunity to make use of the derivative terms of the RBFNN inputs in the presence of constantly fluctuating winds.

Figs. 13a and 13b show the trace plots for the policy parameters during second phase training. After roughly 40 iterations, it is clear that RL-MCMC has learned the policy parameters for the sinusoidal reference. Also there is a converging tendency in the overall return seen in Figure 13c.

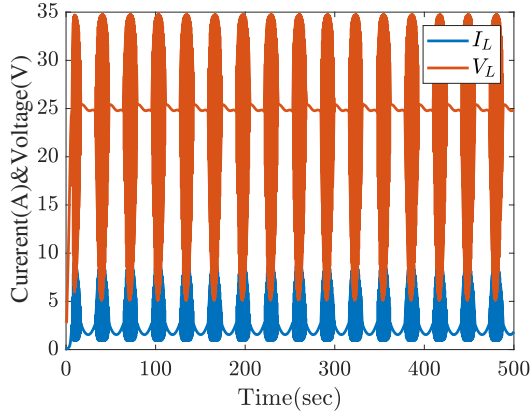




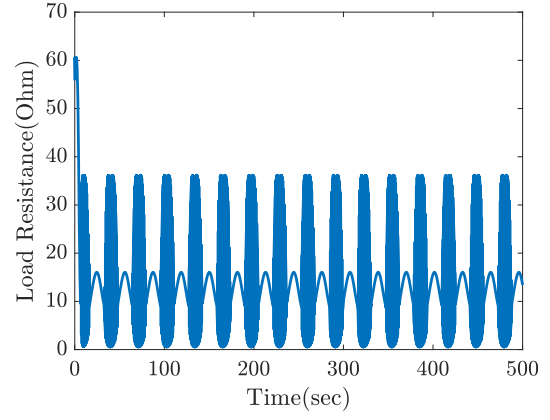
(a) Obtained power



(b) Rotor's angular velocity



(c) Measure current and voltage of the load



(d) Resistance of the load

Figure 12: Time response results for  $P$ ,  $\omega_r$ ,  $V_L$ ,  $I_L$  and  $R_L$  by RL-MCMC at the start of training's second phase using  $\theta_{S1}$ .

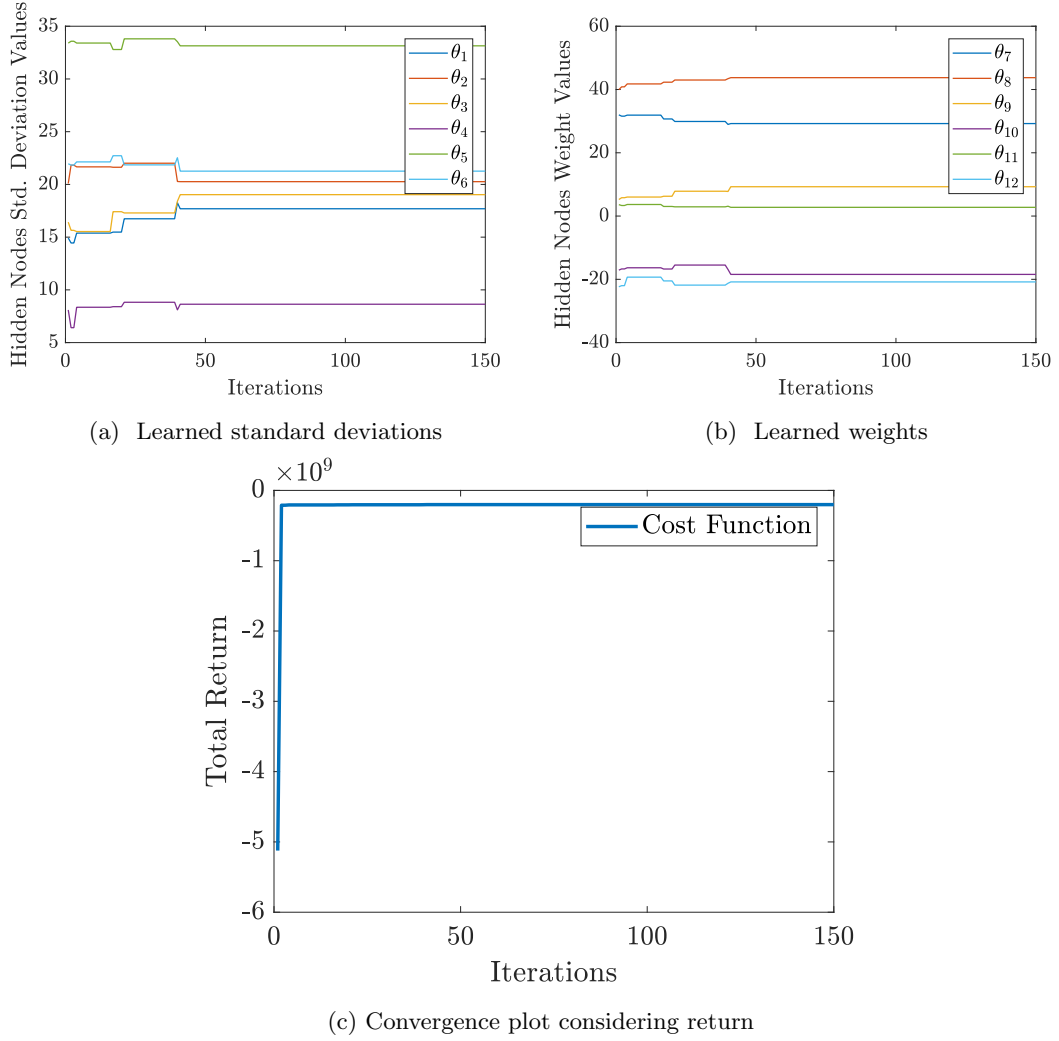


Figure 13: Trace plots of the parameters and their corresponding total return during the second stage of training.

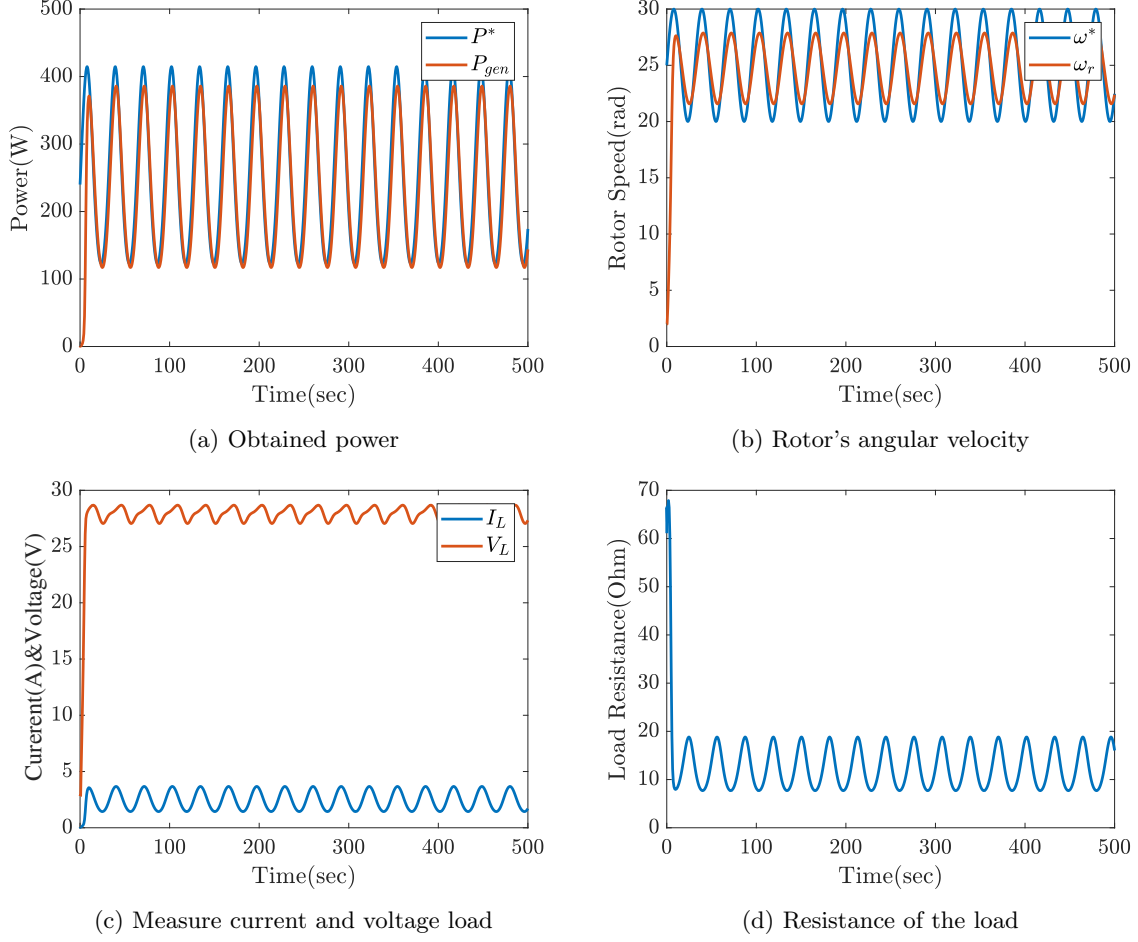


Figure 14: Time response results by RL-MCMC after  $2^{nd}$  stage training, using  $\theta_{S2}$  parameters

Figure 14 displays the results after second stage training using  $\theta_{S2}$  parameters. The rotor speed and output power track the theoretically nominal power of the system, in comparison to Figure 12. As a result, We may conclude that the system's effectiveness has been enhanced with the incorporation of training's second phase. The learned corresponding  $w$  and  $\sigma$  parameters for both phases are given in Table 5.

#### 5.4 The Proposed RL-MCMC and Its Competitor MPPT

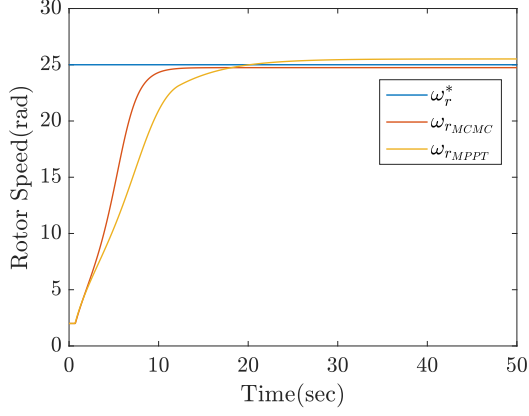
Here, we compare the proposed RL-MCMC for WECS with the widely-used MPPT algorithm with respect to control efficiency and the total capacity of the produced energy. In this section, a comparison between the proposed RL-MCMC for WECS and the commonly used MPPT algorithm considering control efficiency and generated energy. This comparison is carried out through two different scenarios; first, RL-MCMC and MPPT are compared using a step wind (10  $m/s$ ) to illustrate onset control performances,

Table 5: Learned parameters for both  $1^{st}$  and  $2^{nd}$  training phases

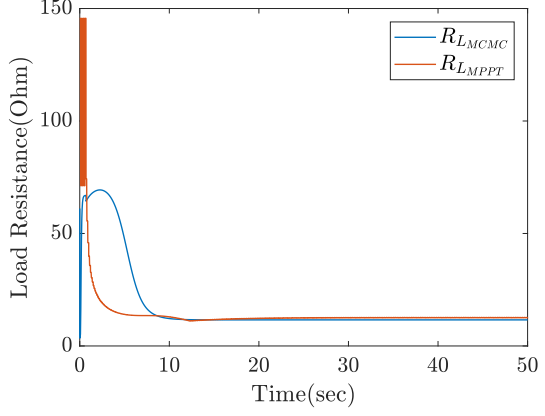
$w_{S1}$	$\sigma_{S1}$	$w_{S2}$	$\sigma_{S2}$
32	14.9	29.2	17.8
40	20.1	43.7	20.3
5.2	16.4	9.3	19
-17.1	8.1	-18.5	8.6
3.6	33.4	2.7	33.3
-22.3	22	-20.8	21.2

Table 6: Classification of the used MPPT with respect to its parameters.

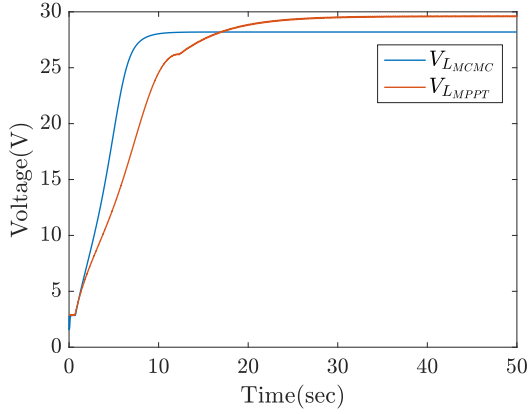
Type	Sampling Time	$\Delta I_{ref}$
$mppt_1$	0.1 s	0.02 A
$mppt_2$	0.1 s	0.01 A



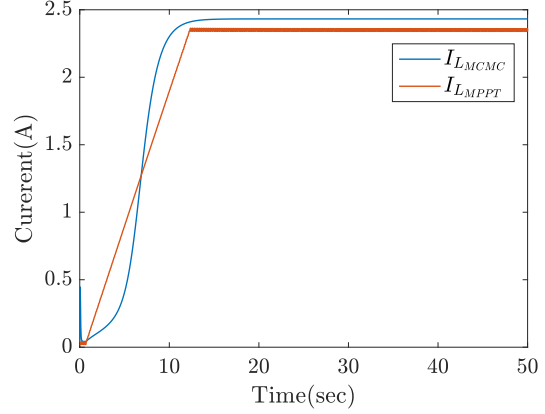
(a) Rotor's nominal speed versus applied algorithms.



(b) Resistance comparison.



(c) Voltages of the load.



(d) Currents of the load

Figure 15: Time response comparisons between MPPT ( $mppt_1$ ) and RL-MCMC using  $\theta_{S2}$ .

and in the second step, the performance in a realistic wind profile is compared. Since MPPT is a greedy algorithm aiming to maximize the instantaneous power, we expect its performance to be inferior. For these comparisons,  $\theta_{S2}$  parameters are used in MCMC, whereas, for MPPT, the parameter set  $mppt_1$ , shown in Table 6, is used. Since it has a higher search rate,  $\Delta I_{ref}$ , it reaches the optimal rotor speed quickly and is suitable for realistic wind profiles, although it will present larger ripple in steady state wind. We also tested another parameter set  $mppt_2$  with smaller  $\Delta I_{ref}$ , designed for stable winds. Its performance will be compared briefly in Table 7.

#### 5.4.1 RL-MCMC and MPPT Subjected to Step Wind Speed

The purpose of this evaluation is to contrast the onset quality of the control strategies. A given step wind as a reference is a practical method of simulating the extreme variations in the speed of wind that provide a significant challenge to WECS. Results of RL-MCMC run with an RBFNN structure (amplitude of 10 m/s for step velocity of wind) set to  $\theta_{S2}$  is analysed in comparison to those of  $mppt_1$  provided in Table 6.

The simulation results of  $\omega_r$ ,  $R_L$ ,  $V_L$ , and  $I_L$  are shown in Figure 15. Selecting a proper  $\omega_r$  is crucial to attain optimal value of  $C_p$ .

The value of  $U_w$  is used in the equation (2) to determine  $\omega_r^*$  rotor's optimum speed.  $\omega_r^*$  relative to

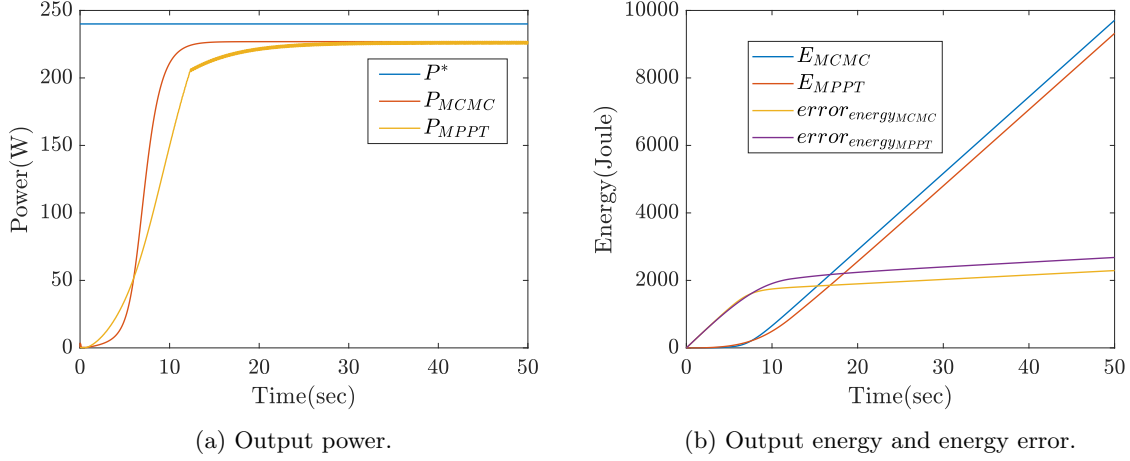


Figure 16: The comparisons for the output power and energy as a result of a step wind (10m/s).

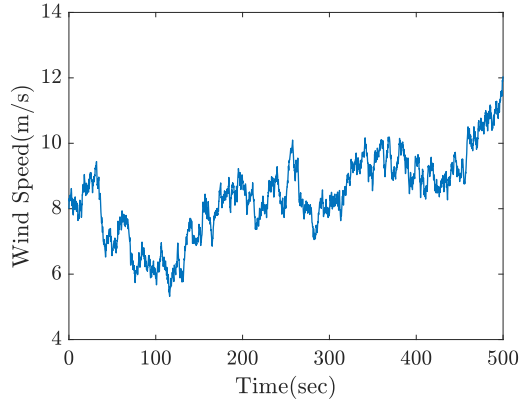


Figure 17: A sample simulated real wind speed  $U_w$  using *Aerospace* toolbox of MATLAB.

MPPT and proposed RL-MCMC time plots ( $\omega_{rMPPT}$ ,  $\omega_{rMCMC}$ ) is compared in Figure 15a. One can readily see that  $\omega_{rMCMC}$  is more in line with  $\omega_r^*$  than  $\omega_{rMPPT}$ . Figure 15c shows that  $V_L$  is proportional to  $\omega_r$ , therefore our findings are in agreement with that. By keeping the load low at first, as demonstrated in Figure 15d, RL-MCMC is able to raise  $I_L$  smoothly and rapidly, making it the clear winner amongst the two control mechanisms. This results in a faster convergence of MCMC to the optimal  $\omega_r^*$  and leads to a more efficient energy output, which was the original goal of this study.

The generated power for RL-MCMC and MPPT are demonstrated in Figure 16a. In steady state, they exhibit a similar performance although the ripple of MPPT output power in steady state is a disadvantage. However, the transient behaviors of these two controllers are significantly different. The total energy and energy error plots shown in Figure 16b clearly shows the difference. MCMC performs better during the transient period and the accumulated extra energy can be seen in the  $E_{MCMC}$  plot. It is expected that for rapidly and continuously changing wind profiles, the difference would be even more significant.

#### 5.4.2 RL-MCMC and MPPT Subjected to Realistic Wind Speed

We evaluate the two approaches using realistic simulated wind conditions. The wind has been generated in MATLAB using the Aerospace Toolbox, where it is characterized as the combination of a variable speed with noise. Figure 17 displays a sample reference wind profile  $U_w$  created from a given wind source. Convergence to the correct value of  $\omega_r$  is the most important factor in determining the best value for  $C_p$ , as was discussed before. The differences in the responses between  $\omega_{rMPPT}$  and  $\omega_{rMCMC}$ , are depicted in Figure 18. According to this figure,  $\omega_{rMCMC}$  is more closely maintained at  $\omega_r^*$  whereas, MPPT could not manage to generate a speed close to optimum. Figure 19 shows the response of controlled resistance of the load for the RL-MCMC and MPPT where former is more responsive to variations in the speed of

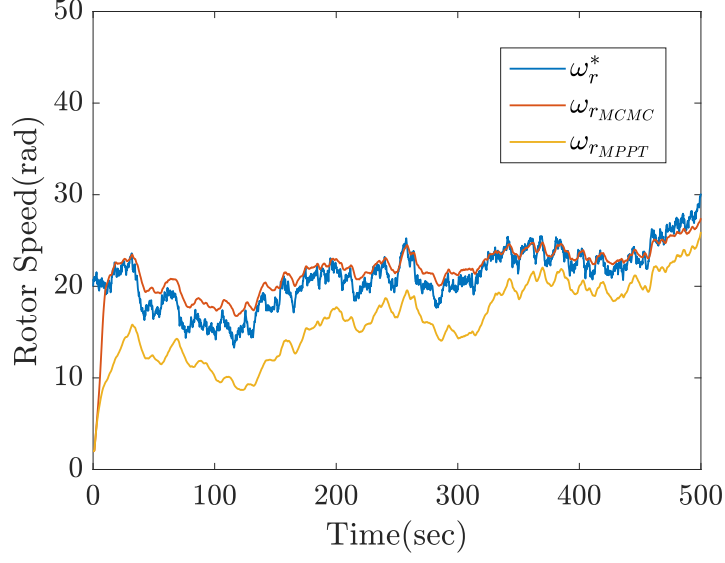


Figure 18: Comparisons for the speed of rotor under a real simulated wind.

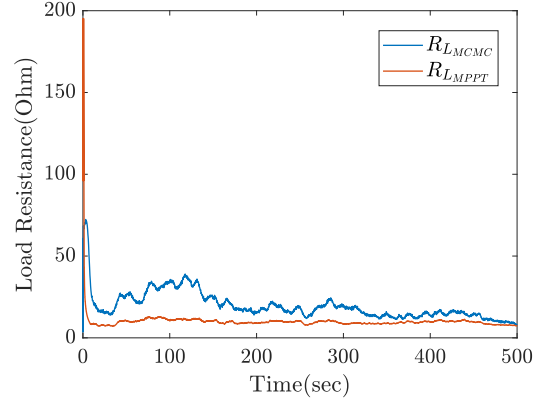
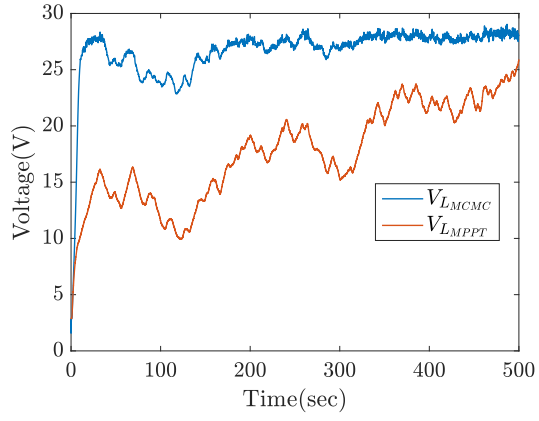


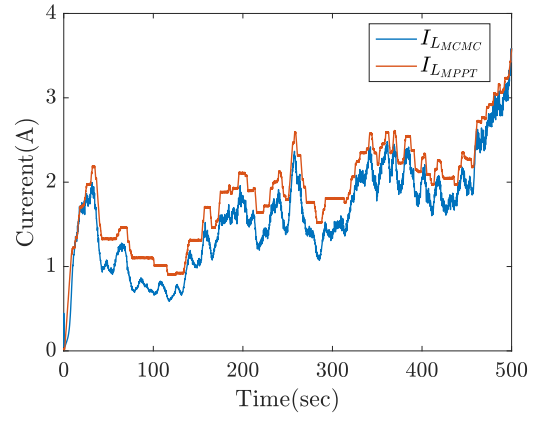
Figure 19: The Responses of the resistance in the load for simulated real wind.

wind.

The resulting response of the current and voltage in the load also are shown in Figure 20. In Fig. 18, the wind speed does not have a definitive trend. We can see that  $\omega_{rMCMC}$  and  $V_{LMCMC}$  follow the wind speed closely, and thus they can keep a good  $C_p$  value (in synchronous generators, output voltage is generally proportional to rotor speed omitting inductance and resistance effects). However, it can be seen that  $V_{LMPPT}$  has a definitive increasing trend which suggests that it cannot keep a good  $C_p$ .



(a) Voltage of load



(b) Current of load

Figure 20: Comparisons between the current and voltages of the load using a real simulated wind.

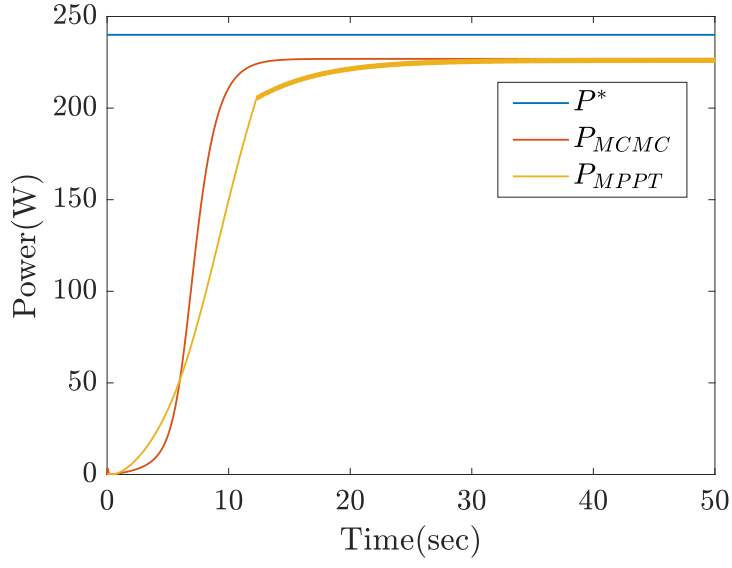


Figure 21: Comparisons for the power with a real simulated wind.

It is evident from Figure 21 that the RL-MCMC's generated power can track its nominal value better than its counterpart. Figure 22 displays the cumulative energy generated, showing that RL-MCMC can provide more energy and keeps rising above that of MPPT. When it comes to the error comparison, MPPT has a greater error between the ideal and actual output energy.



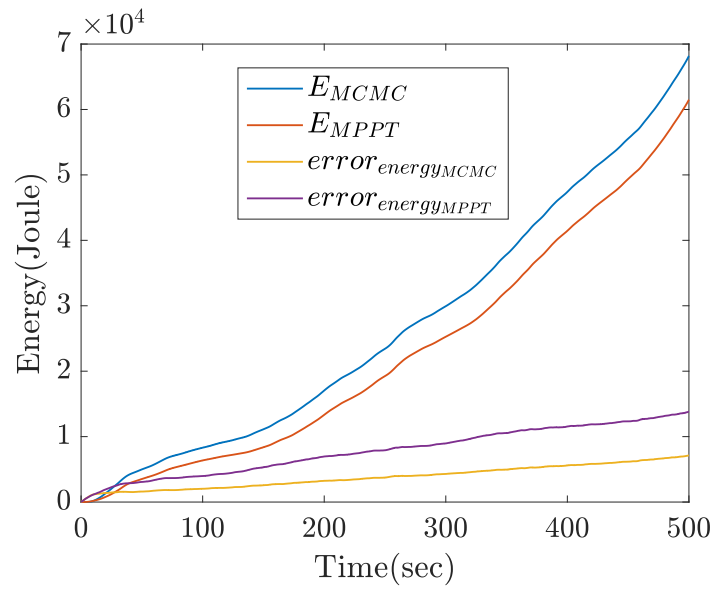


Figure 22: Comparisons for the generated energy with a real simulated wind

Table 7: Results of the energy output **error**  $e$  from the optimal (Joules).

Number of tests	Proposed RL-MCMC	$mppt_1$	$mppt_2$
1	8117.7	19844.5	12511.7
2	8254.7	9933.5	32410.5
3	8671.9	9654.2	11929.7
4	5917.6	35108.9	8024.1
5	7726.5	33325.8	38513.7
6	7695.6	31365.4	45678.7
7	7757.4	45690.7	8003.5
8	7787.8	57123.1	7802.2
9	8114.1	22900.9	13489.9
10	8117.4	17834.3	10523.4

Table 8: Mean and standard deviation of the energy output-errors (Joules).

Controller	Mean	SD
RL-MCMC	7816	732
$mppt_1$	28278	15309
$mppt_2$	23889	27411

The statistical consistency of the two methods were also investigated. Since MCMC approaches have a statistical background, it is expected that the results be statistically more consistent. We repeated this simulation 10 times through different real wind waves and measured total energy’s mean and standard deviation (SD) for the controllers. These simulations were performed for 3 controllers including  $mppt_2$  as well as RL-MCMC and  $mppt_1$ . The results are listed in Table 7. It is clear that MPPTs have nearly four times the energy output-error of the proposed algorithm. Furthermore, Table 8 shows that the MPPTs’ SD is high, indicating that their performance is highly sensitive to variations in wind speed, in contrast to RL-MCMC’s reliable performance in a wide range of actual wind conditions.

## 6 Conclusion

Conventional controllers have inferior performance because of properties such as the lack of long term optimization or the requirement of linearization of the plant model which prevents them from performing well in changing wind profiles. Moreover, they may be geared towards maximizing instantaneous power output which does not result in maximum energy output. Output energy optimization of WECS is a complex problem with an complex objective function which precludes the use of gradient based algorithms. To tackle all of these problems and motivated by the exploration-exploitation dilemma, we have developed an RL-MCMC algorithm that combines the strengths of both the gradient-free Bayesian MCMC and RL algorithms. We use MCMC sampling method that is capable of exploring the high-reward regions of the policy space (benefiting from the RL algorithm). Since the policy space is explored in a non-contiguous manner, different regions can be visited and the probability of discovering better performing regions always exists. Our proposed Algorithm 1 does not converge to a single point. Instead, the policy parameters are guaranteed to follow the desired posterior distribution. The proposed algorithm employs an RBFNN as an approximator that learns to control the unknown nonlinear VAWT dynamics, responds to arbitrary wind profiles, and provides a nonlinear controller that manipulates the electrical load power reference as a control signal. When applied to learning VAWT’s nonlinear model, we found that the suggested RL-MCMC technique achieves promising results. The system’s performance was bootstrapped such that it could eventually handle actual wind shapes by first applying step and later sine waveform as the reference winds. We demonstrated that, in terms of overall energy production, the proposed approach outperforms its conventional counterpart MPPT. For the real wind, RL-MCMC showed to be 89 percent energy-efficient, whereas this number for MPPT is 78 percent. To illustrate the reliability of the proposed control method, in terms of energy output, we averaged the results of 10 different simulations of several real winds. As may be seen in Table 7 however, MPPT was more erratic.

As a future concern, we aim to incorporate a final training stage in a physical setup, where recorded

real wind data is applied to the VAWT and corresponding final weights are learned. Since the learning can be performed on collected data with batch processing, it is possible to complete this final step using even a simple microcomputer.

## References

- Ağababaoğlu, A., 2019. Bayesian reinforcement learning with MCMC to maximize energy output of vertical axis wind turbine. Master's thesis. Sabancı University. Istanbul.
- Aghaei, V.T., Onat, A., Yıldırım, S., 2018. A markov chain monte carlo algorithm for bayesian policy search. *Systems Science & Control Engineering* 6, 438–455. doi:10.1080/21642583.2018.1528483.
- Andrieu, C., de Freitas, N., Doucet, A., Jordan, M.I., 2003. An introduction to MCMC for machine learning. *Machine Learning* 50, 5–43.
- Aourir, J., Locment, F., 2020. Limited power point tracking for a small-scale wind turbine intended to be integrated in a dc microgrid. *Applied Sciences* 10. doi:10.3390/app10228030.
- Asghar, A.B., Liu, X., 2018. Adaptive neuro-fuzzy algorithm to estimate effective wind speed and optimal rotor speed for variable-speed wind turbine. *Neurocomputing* 272, 495–504. doi:https://doi.org/10.1016/j.neucom.2017.07.022.
- Bemporad, A., 2015. Explicit model predictive control., in: Baillieul, J., Samad, T. (Eds.), *Encyclopedia of Systems and Control*. Springer.
- Brochu, E., Cora, V.M., de Freitas, N., 2010. A tutorial on bayesian optimization of expensive cost functions, with application to active user modeling and hierarchical reinforcement learning. *CoRR* abs/1012.2599. URL: <http://arxiv.org/abs/1012.2599>, arXiv:1012.2599.
- Bui, V.H., Nguyen, T.T., Kim, H.M., 2020. Distributed operation of wind farm for maximizing output power: A multi-agent deep reinforcement learning approach. *IEEE Access* 8, 173136–173146. doi:10.1109/ACCESS.2020.3022890.
- Chang, K.H., Hong, L.J., Wan, H., 2013. Stochastic trust-region response-surface method (strong) - a new response-surface framework for simulation optimization. *INFORMS J. Comput.* 25, 230–243.
- Cheng, M., Zhu, Y., 2014. The state of the art of wind energy conversion systems and technologies: A review. *Energy Conversion and Management* 88, 332–347. doi:https://doi.org/10.1016/j.enconman.2014.08.037.
- Chojaa, H., Derouich, A., Chehaidia, S.E., Zamzoum, O., Taoussi, M., Elouatouat, H., 2021. Integral sliding mode control for dfig based wecs with mppt based on artificial neural network under a real wind profile. *Energy Reports* 7, 4809–4824. doi:https://doi.org/10.1016/j.egyr.2021.07.066.
- Da Rosa, A.V., Ordóñez, J.C., 2021. *Fundamentals of renewable energy processes*. Academic Press.
- Dali, A., Abdelmalek, S., Bakdi, A., Bettayeb, M., 2021. A new robust control scheme: Application for mpp tracking of a pmsg-based variable-speed wind turbine. *Renewable Energy* 172, 1021–1034. doi:https://doi.org/10.1016/j.renene.2021.03.083.
- Derman, E., Mankowitz, D., Mann, T., Mannor, S., 2020. A bayesian approach to robust reinforcement learning, in: Adams, R.P., Gogate, V. (Eds.), *Proceedings of The 35th Uncertainty in Artificial Intelligence Conference*, PMLR. pp. 648–658.
- Durrant-Whyte, H., Roy, N., Abbeel, P., 2012. Learning to Control a Low-Cost Manipulator Using Data-Efficient Reinforcement Learning. pp. 57–64.
- Gal, Y., Ghahramani, Z., 2016. Dropout as a bayesian approximation: Representing model uncertainty in deep learning, in: *Proceedings of the 33rd International Conference on International Conference on Machine Learning - Volume 48*, JMLR.org. pp. 1050–1059.
- García, C.E., Prett, D.M., Morari, M., 1989. Model predictive control: Theory and practice—a survey. *Automatica* 25, 335 – 348. doi:https://doi.org/10.1016/0005-1098(89)90002-2.

- Gebraad, P.M.O., van Wingerden, J.W., 2015. Maximum power-point tracking control for wind farms. *Wind Energy* 18, 429–447. doi:<https://doi.org/10.1002/we.1706>.
- Horvat, T., Spudić, V., Baotić, M., 2012. Quasi-stationary optimal control for wind farm with closely spaced turbines, in: 2012 Proceedings of the 35th International Convention MIPRO, pp. 829–834.
- Jia, Y., Ma, S., 2021. A coach-based bayesian reinforcement learning method for snake robot control. *IEEE Robotics and Automation Letters* 6, 2319–2326. doi:10.1109/LRA.2021.3061372.
- Karthik, R., Harsh, H., Pavan Kumar, Y.V., John Pradeep, D., Pradeep Reddy, C., Kannan, R., 2022. Modelling of neural network-based mppt controller for wind turbine energy system, in: Suhag, S., Mahanta, C., Mishra, S. (Eds.), *Control and Measurement Applications for Smart Grid*, Springer Nature Singapore, Singapore. pp. 429–439.
- Keighobadi, J., Mohammadian KhalafAnsar, H., Naseradinmousavi, P., 2022. Adaptive neural dynamic surface control for uniform energy exploitation of floating wind turbine. *Applied Energy* 316, 119132. doi:<https://doi.org/10.1016/j.apenergy.2022.119132>.
- Khorsand, I., Kormos, C., MacDonald, E.G., Crawford, C., 2015. Wind energy in the city: An interurban comparison of social acceptance of wind energy projects. *Energy Research & Social Science* 8, 66–77. doi:<https://doi.org/10.1016/j.erss.2015.04.008>.
- Kofinas, P., Doltsinis, S., Dounis, A., Vouros, G., 2017. A reinforcement learning approach for mppt control method of photovoltaic sources. *Renewable Energy* 108, 461–473. doi:<https://doi.org/10.1016/j.renene.2017.03.008>.
- Lasheen, M., Bendary, F., Sharaf, A., M. El-Zoghby, H., 2015. Maximum power point tracking of a wind turbine driven by synchronous generator connected to an isolated load using genetic algorithm. *Journal of Electrical Engineering* 15, 21.
- Laxman, B., Annamraju, A., Srikanth, N.V., 2021. A grey wolf optimized fuzzy logic based mppt for shaded solar photovoltaic systems in microgrids. *International Journal of Hydrogen Energy* 46, 10653–10665. doi:<https://doi.org/10.1016/j.ijhydene.2020.12.158>.
- Levine, S., Finn, C., Darrell, T., Abbeel, P., 2016. End-to-end training of deep visuomotor policies. *J. Mach. Learn. Res.* 17, 1334–1373.
- Li, X., Wen, H., Hu, Y., Jiang, L., 2019. Drift-free current sensorless mppt algorithm in photovoltaic systems. *Solar Energy* 177, 118–126. doi:<https://doi.org/10.1016/j.solener.2018.10.066>.
- Lin, D., Li, X., Ding, S., Wen, H., Du, Y., Xiao, W., 2021. Self-tuning mppt scheme based on reinforcement learning and beta parameter in photovoltaic power systems. *IEEE Transactions on Power Electronics* 36, 13826–13838. doi:10.1109/TPEL.2021.3089707.
- Marco, A., Berkenkamp, F., Hennig, P., Schoellig, A.P., Krause, A., Schaal, S., Trimpe, S., 2017. Virtual vs. Real: Trading off simulations and physical experiments in reinforcement learning with Bayesian optimization, in: *Proceedings of the IEEE International Conference on Robotics and Automation (ICRA)*, IEEE, Piscataway, NJ, USA. pp. 1557–1563.
- Ngo, Q.V., Yi, C., Nguyen, T.T., 2020. The maximum power point tracking based-control system for small-scale wind turbine using fuzzy logic. *International Journal of Electrical and Computer Engineering* 10, 3927–3935.
- Norouzi, A., Shahpouri, S., Gordon, D., Winkler, A., Nuss, E., Abel, D., Andert, J., Shahbakhti, M., Koch, C.R., 2022. Deep learning based model predictive control for compression ignition engines. *Control Engineering Practice* 127, 105299. doi:<https://doi.org/10.1016/j.conengprac.2022.105299>.
- Onol, A., Sancar, U., Onat, A., Yesilyurt, S., 2015. Model predictive control for energy maximization of small vertical axis wind turbines, in: *Dynamic Systems and Control Conference*, American Society of Mechanical Engineers. p. V001T05A003.
- Ouyang, Y., Sun, C., Dong, L., 2022. Actor–critic learning based coordinated control for a dual-arm robot with prescribed performance and unknown backlash-like hysteresis. *ISA Transactions* 126, 1–13. doi:[doi:10.1016/j.isatra.2021.08.005](https://doi.org/10.1016/j.isatra.2021.08.005).

- Park, J., Law, K.H., 2015. Cooperative wind turbine control for maximizing wind farm power using sequential convex programming. *Energy Conversion and Management* 101, 295–316. doi:[doi.org/10.1016/j.enconman.2015.05.031](https://doi.org/10.1016/j.enconman.2015.05.031).
- Park, J., Law, K.H., 2016. Bayesian ascent: A data-driven optimization scheme for real-time control with application to wind farm power maximization. *IEEE Transactions on Control Systems Technology* 24, 1655–1668. doi:[10.1109/TCST.2015.2508007](https://doi.org/10.1109/TCST.2015.2508007).
- Pautrat, R., Chatzilygeroudis, K.I., Mouret, J., 2018. Bayesian optimization with automatic prior selection for data-efficient direct policy search, in: *ICRA, IEEE*. pp. 7571–7578.
- Peters, J., Schaal, S., 2008. Natural actor-critic. *Neurocomputing* 71, 1180 – 1190. doi:<https://doi.org/10.1016/j.neucom.2007.11.026>. progress in Modeling, Theory, and Application of Computational Intelligence.
- Powell, M.J.D., 2008. Developments of newuoa for minimization without derivatives. *IMA Journal of Numerical Analysis* 28, 649–664. doi:[10.1093/imanum/drm047](https://doi.org/10.1093/imanum/drm047).
- Prince, M.K.K., Arif, M.T., Gargoom, A., Oo, A.M.T., Haque, M.E., 2021. Modeling, parameter measurement, and control of pmsg-based grid-connected wind energy conversion system. *Journal of Modern Power Systems and Clean Energy* 9, 1054–1065. doi:[10.35833/MPCE.2020.000601](https://doi.org/10.35833/MPCE.2020.000601).
- Rana, K., Dasagi, V., Haviland, J., Talbot, B., Milford, M., Sünderhauf, N., 2021. Bayesian controller fusion: Leveraging control priors in deep reinforcement learning for robotics. *CoRR abs/2107.09822*. [arXiv:2107.09822](https://arxiv.org/abs/2107.09822).
- Rios, L.M., Sahinidis, N.V., 2013. Derivative-free optimization: a review of algorithms and comparison of software implementations. *Journal of Global Optimization* 56, 1247–1293.
- Sancar, U., 2015. Hardware-in-the-loop simulations and control designs for a vertical axis wind turbine. Master’s thesis. Sabancı University. Istanbul.
- Seyyedabbasi, A., Kiani, F., 2021. I-gwo and ex-gwo: improved algorithms of the grey wolf optimizer to solve global optimization problems. *Engineering with Computers* 37, 509–532.
- Sitharthan, R., Karthikeyan, M., Sundar, D.S., Rajasekaran, S., 2020. Adaptive hybrid intelligent mppt controller to approximate effectual wind speed and optimal rotor speed of variable speed wind turbine. *ISA Transactions* 96, 479–489. doi:<https://doi.org/10.1016/j.isatra.2019.05.029>.
- Soleimanzadeh, M., Wisniewski, R., 2011. Controller design for a wind farm, considering both power and load aspects. *Mechatronics* 21, 720–727. doi:<https://doi.org/10.1016/j.mechatronics.2011.02.008>.
- Song, D., Yang, J., Dong, M., Joo, Y.H., 2017. Model predictive control with finite control set for variable-speed wind turbines. *Energy* 126, 564 – 572. doi:<https://doi.org/10.1016/j.energy.2017.02.149>.
- Sutton, R.S., Barto, A.G., 1998. Reinforcement Learning: An Introduction. Adaptive computation and machine learning. MIT Press, Cambridge, MA, USA.
- Syahputra, R., Soesanti, I., 2019. Performance improvement for small-scale wind turbine system based on maximum power point tracking control. *Energies* 12. doi:[10.3390/en12203938](https://doi.org/10.3390/en12203938).
- Tasneem, Z., Al Noman, A., Das, S.K., Saha, D.K., Islam, M.R., Ali, M.F., R Badal, M.F., Ahamed, M.H., Moyeen, S.I., Alam, F., 2020. An analytical review on the evaluation of wind resource and wind turbine for urban application: Prospect and challenges. *Developments in the Built Environment* 4, 100033. doi:<https://doi.org/10.1016/j.dibe.2020.100033>.
- Tavakol Aghaei, V., Ağababaoğlu, A., Yıldırım, S., Onat, A., 2021. A real-world application of markov chain monte carlo method for bayesian trajectory control of a robotic manipulator. *ISA Transactions* doi:<https://doi.org/10.1016/j.isatra.2021.06.010>.
- Tripathi, S., Tiwari, A., Singh, D., 2015. Grid-integrated permanent magnet synchronous generator based wind energy conversion systems: A technology review. *Renewable and Sustainable Energy Reviews* 51, 1288–1305. doi:<https://doi.org/10.1016/j.rser.2015.06.060>.

- Tummala, A., Velamati, R.K., Sinha, D.K., Indraj, V., Krishna, V.H., 2016. A review on small scale wind turbines. *Renewable and Sustainable Energy Reviews* 56, 1351 – 1371. doi:<https://doi.org/10.1016/j.rser.2015.12.027>.
- Wei, C., Zhang, Z., Qiao, W., Qu, L., 2016. An adaptive network-based reinforcement learning method for mppt control of pmsg wind energy conversion systems. *IEEE Transactions on Power Electronics* 31, 7837–7848. doi:10.1109/TPEL.2016.2514370.
- Wilson, A., Fern, A., Tadepalli, P., 2014. Using trajectory data to improve bayesian optimization for reinforcement learning. *J. Mach. Learn. Res.* 15, 253–282. URL: <http://dblp.uni-trier.de/db/journals/jmlr/jmlr15.html#WilsonFT14>.
- Yaakoubi, A., Amhaimar, L., Attari, K., Harrak, M., Halaoui, M., Asselman, A., 2019. Non-linear and intelligent maximum power point tracking strategies for small size wind turbines: Performance analysis and comparison. *Energy Reports* 5, 545–554. doi:<https://doi.org/10.1016/j.egy.2019.03.001>.
- Yang, B., Yu, T., Shu, H., Zhang, Y., Chen, J., Sang, Y., Jiang, L., 2018. Passivity-based sliding-mode control design for optimal power extraction of a pmsg based variable speed wind turbine. *Renewable Energy* 119, 577–589. doi:<https://doi.org/10.1016/j.renene.2017.12.047>.
- Youssef, A.R., Mousa, H.H., Mohamed, E.E., 2020. Development of self-adaptive p&o mppt algorithm for wind generation systems with concentrated search area. *Renewable Energy* 154, 875–893. doi:<https://doi.org/10.1016/j.renene.2020.03.050>.
- Zhang, B., Hu, W., Li, J., Cao, D., Huang, R., Huang, Q., Chen, Z., Blaabjerg, F., 2020. Dynamic energy conversion and management strategy for an integrated electricity and natural gas system with renewable energy: Deep reinforcement learning approach. *Energy Conversion and Management* 220, 113063. doi:<https://doi.org/10.1016/j.enconman.2020.113063>.
- Özgün Önel, A., 2016. Modeling, hardware-in-the-loop simulations and control design for a vertical axis wind turbine with high solidity. Master’s thesis. Sabancı University. Istanbul.